

1 **Mixing state of black carbon at different atmospheres in north and southwest** 2 **China**

3 Gang Zhao¹, Tianyi Tan¹, Shuya Hu¹, Zhuofei Du¹, Dongjie Shang¹, Zhijun Wu^{1,2}, Song
4 Guo^{1,2}, Jing Zheng¹, Wenfei Zhu¹, Mengren Li¹, Limin Zeng^{1,2}, Min Hu^{1, 2*}

5 1 State Key Joint Laboratory of Environmental Simulation and Pollution Control,
6 International Joint Laboratory for Regional Pollution Control, Ministry of Education,
7 College of Environmental Sciences and Engineering, Peking University, Beijing,
8 100871, China

9 2 Collaborative Innovation Center of Atmospheric Environment and Equipment
10 Technology, Nanjing University of Information Science & Technology, Nanjing, China

11 ***Correspondence author:** Min Hu (minhu@pku.edu.cn)

12 **Abstract**

13 Large uncertainties remain when estimating the radiative forcing by black carbon
14 (BC) because the corresponding microphysical properties have not been well addressed.
15 In this study, the BC size distributions were studied based on three different field
16 campaigns at an urban site, a suburban site, and a background site in China using a
17 single particle soot photometer (SP2) in tandem with a differential mobility diameter.
18 Measurement results indicate that the BC particles were composed of either thinly or
19 thickly coated aerosols. The mean number fractions of the thinly coated BC aerosols
20 were 51%, 67%, and 21% for the urban, suburban, and background sites, respectively.
21 The corresponding thickly coated (thinly coated) core mass median diameters were 187
22 nm (154 nm), 182 nm (146 nm), and 238 nm (163 nm), respectively. The mean diameter
23 of the thickly coated BC-containing aerosols was larger than that of the thinly coated

24 BC-containing aerosols, while the mean BC core diameter of the thickly coated BC-
25 containing aerosols was smaller than that of the thinly coated BC-containing aerosols.
26 About 10% of the BC-containing aerosols with the BC core are attached to the other
27 non-BC components, which were mainly generated by coagulation between the BC and
28 non-BC components. The measurement results in our study can be further used in
29 modeling studies to help with constraining the uncertainties of the BC radiative effects.

30 **Introduction**

31 Black carbon (BC) plays an important role in the climate system by absorbing solar
32 radiation (Ramanathan and Carmichael, 2008), interacting with the cloud (Roberts et al.,
33 2008), and changing the albedo of the snow (Menon et al., 2002). It is the second most
34 important aerosol component after carbon dioxide, contributing to global warming
35 (Bond et al., 2013). The solar absorption of BC has a significant influence on the
36 development of the boundary layer and then aggravates the air pollution (Ding et al.,
37 2016). The turbulence in the atmospheric boundary layer can be suppressed due to the
38 existence of BC (Wilcox et al., 2016). The BC also plays a remarkable role in driving
39 the formation and trend of regional haze (Zhang et al., 2020).

40 BC is mainly generated by the incomplete combustion of biofuels and fossil fuels
41 (Bond and Bergstrom, 2006). After emission, the morphology of BC transforms from
42 fractal to spherical and subsequently grows to a fully compact particle with other
43 chemical components coating it (Peng et al., 2016). During the aging process, the BC
44 optical properties change significantly up to a factor of 3 and then the corresponding
45 magnitude of climate forcing contributed by BC is increased by up to a factor of 2
46 (Zhang et al., 2008). Large uncertainties remain in estimating the BC radiative effects
47 due to the large variation in BC microphysical properties, such as size distributions and
48 mixing states during the aging process (Zhao et al., 2019; Moffet et al., 2016; Matsui et

49 al., 2018). Therefore, characterizing the differences in size distributions and mixing
50 states between the thinly and thickly coated BC particles can help better constrain the
51 uncertainties of BC aerosol radiative effects. To our best understanding, few studies
52 have specified the mixing states and size distributions of both the thinly and thickly
53 coated BC aerosols.

54 The thickly coated BC particles can also be classified into two morphological types:
55 bare BC on the surface of non-BC particles or partially coated by non-BC particles
56 (attached type) and BC embedded within or coated by non-BC components (coated
57 type). With the same amount of non-BC components, the mass absorption cross-sections
58 of BC by the attached type are much smaller than those by the coated type (Moteki and
59 Kondo, 2008; Moteki and Kondo, 2010; Moteki et al., 2014). Therefore, the impact of
60 BC on climate can be better estimated when accurately identifying the two types of
61 ambient BC-containing particles. Observations are required to constrain the spatial and
62 temporal microphysical properties of the atmospheric BC.

63 The single-particle soot photometer (SP2) is always used to measure the mixing
64 states and size distributions of ambient BC particles. In the previous study, advanced
65 technology was used to study the coating over different BC core size diameters on the
66 ground (Liu et al., 2019a) and for vertical profiles (Ding et al., 2019). The measured
67 signals from SP2 can be used to distinguish the BC-containing aerosols as thinly and
68 thickly coated ones. The measured results can also be employed to distinguish the BC-
69 containing particles between attached and coated types, which were described in detail
70 in the methodology part.

71 In this study, the tandem SP2 and differential mobility analyzer (DMA) was
72 employed at an urban site, a suburban site, and a background site in China to investigate
73 the microphysical properties of the BC particles. The size distributions and mixing states

of both the thinly coated and thickly coated BC aerosols at different atmospheres were characterized. We also investigated the corresponding morphology properties of the BC-containing aerosols. The measured microphysical properties provide the basis for future modeling studies of the BC radiative effects in different environments in China.

2 Methodology

2.1 Measurement sites

The measurements were conducted at three different atmospheric sites in China, namely the urban site of Peking University Urban Atmosphere Environment Monitoring Station (PKU, 39.9°N, 116.1°E, 58m a.s.l) in Beijing between 20 January and 4 February 2016, the suburban site of Changping (CP, 40.3°N, 116.2°E, 70m a.s.l) in Beijing between 15 May and 5 June 2016, and the background site of Lijiang (LJ, 27.2°N, 100.2°E, 3410 m a.s.l) in Yunnan Province between 22 March and 4 April 2015. The PKU site is located northwest of Beijing. This site could characterize the air pollution of urban Beijing (Hu et al., 2017; Hu et al., 2021b). The CP site locates in the northwest of the Beijing urban area, representing a regional atmosphere (Zhao et al., 2021; Wang et al., 2019b). The LJ site represents the background areas, located in the Mountain Yulong, in the Yunnan Province of China (Shang et al., 2018; Zheng et al., 2017; Wang et al., 2019a). The aerosol optical depth at the wavelength of 550 nm during the year 2020 indicated that the LJ site was very clean and the PKU and CP sites were more polluted as shown in Fig. S1 in the supplement.

2.2 Instruments

2.2.1 DMA-SP2 system

As for the SP2, the continuous Nd: YAG laser beam with the wavelength of 1064 nm is generated intensively in the instrument chamber. When the BC-containing particles pass through the laser beam, they absorb the radiation and then are heated to around 3500-5000 K. The intensity of the emitted incandescent light from the heated BC particle is then transformed to the BC mass concentration. The scattering signals of the BC particle are recorded to estimate the BC particle mixing state.

In this study, the SP2 (Droplet Measurement Technology, Inc., USA) was placed after the DMA (Model 3081, TSI, USA) to measure the size-resolved BC mixing states, and the instrument setup is schematically shown in Fig. S2. The DMA was set to scan the aerosol over the size range between 12.3 and 697 nm every five minutes. The flow rate leading to the SP2 and the condensation particle counter (CPC, Model 3776, TSI, USA) were 0.12 and 0.28 L/min, respectively. The sheath flow of the DMA was 4 L/min.

The Aquadag was used to calibrate the measured incandescence signal of the SP2 using the DMA-SP2 system. The formula from Gysel et al. (2011) was used to convert the mobility diameter into the mass of Aquadag. A correction factor of 0.75 was applied to account for the different response sensitivity of SP2 to Aquadag and ambient BC (Moteki et al., 2010).

In this study, the coating thickness of the BC-containing aerosols was calculated by the difference between the total mobility diameter measured by the DMA and the optical equivalent diameters of the BC core. Details of calculating the optical equivalent coating thickness can refer to Zhang et al. (2018b) and can be found in section 3 in the supplementary material.

2.2.2 Other instruments

119 The submicron particles (PM_{10}) chemical compositions were measured using a high-
120 resolution time-of-flight aerosol mass spectrometer (AMS; Aerodyne Research Inc.,
121 Billerica, MA, USA). The data processing software PIKA (version 1.16) was used for
122 data analysis. The positive matrix factorization (PMF) analysis was conducted for the
123 source appointment of the organic aerosols (Ulbrich et al., 2009). More details on the
124 measurement of the aerosol chemical compositions and data processing can be found in
125 Zheng et al. (2017).

126 The mass concentrations of O_3 were measured using UV absorption (model 49i,
127 Thermo Fischer Inc. USA) with a time resolution of 1 minute. The mass concentrations
128 of NO and NO_2 were measured using the chemiluminescence technique (NO- NO_2 - NO_x
129 Analyzer, Model 42i, Thermo Scientific, USA). The mass concentrations of SO_2 were
130 measured using the ultraviolet fluorescence method (SO_2 analyzer, model 43i-TLE,
131 Thermo Scientific, USA). The temperature (T), relative humidity (RH), wind speed
132 (WS), and wind direction (WD) were monitored continuously during these campaigns.

133 **2.3 Methodology**

134 For the BC-containing aerosol, there is a lag between the peak time of the scattering
135 and the incandescence signal (Metcalf et al., 2012). The lag time between the peak
136 scattering signal and the peak incandescence signal can be employed to describe the
137 coating thickness (Moteki and Kondo, 2007; Schwarz et al., 2006) and further used to
138 distinguish the BC-containing aerosols as thinly and thickly coated ones. Despite that,
139 the time-lag method may not effectively distinguish the BC particles between fresh or
140 aged ones because some BC particles are sourced from biomass burning (Schwarz et al.,
141 2008b) and solid fuel burning (Liu et al., 2014; Liu et al., 2019b) initially have a higher
142 coating and were not aged ones. However, the lag-time probability distribution at our
143 measurement sites shows two modes which will be shown in section 3.2, and thus the

lag-time can be used to efficiently distinguish the BC-containing aerosols as thinly and thickly coated ones.

For the thickly coated BC particles, the measured scattering and incandescence signal can also be employed to distinguish the BC-containing particles as attached and coated types (Moteki et al., 2014) by calculating the time-dependent scattering cross-sections of BC-containing particles (Moteki and Kondo, 2007). For the coated type, all of the coating material will evaporate and the scattering cross-sections will decrease to zero after passing through the laser beam, while the scattering cross-section of the attached BC-containing aerosol will not decrease to zero (Moteki and Kondo, 2008). The method adopted by Dählkötter et al. (2014) was employed here to characterize the morphology of the BC-containing aerosols. Details of distinguishing the BC-containing particles as attached and coated types can also refer to section 4 in the supplementary materials.

3 Results and discussions

3.1 Overview of the measurement results in different atmospheres

The time series of the measurement results are shown in Fig. S6, Fig. S7, and Fig. S8 for the PKU, CP, and LJ sites, respectively. For the PKU site, the wind was mainly from the north and the wind speed was low with a mean value of 2.2 m/s. The ambient atmosphere was very dry with a mean RH of 27.6%, with minimum and maximum values of 5.8% and 72.6%, respectively. The temperature in the winter in Beijing had a mean value of 0.8 °C between -5.9 °C and 9.2 °C. The mean mass concentration of PM_{2.5} was $49.3 \pm 55.4 \mu\text{g}/\text{m}^3$. The concentration of SO₂ and NO_x (NO_x=NO + NO₂) had the same trends as PM_{2.5}, with mean values of 16.3 ± 11.9 ppb and 68.2 ± 63.4 ppb, respectively. The O₃ concentration is anti-correlated with PM_{2.5}. For the suburban site

168 CP, the wind showed obvious diurnal cycles with high-speed west wind during the day
169 and low-speed east wind during the night. The mean wind speed was 2.4 ± 1.6 m/s. The
170 RH during the campaign was $38.8 \pm 16.0\%$, with a maximum value of 80.5%. The
171 temperature during the campaign was 21.8 ± 5.2 °C with a maximum value of 33.2 °C.
172 As for the NO_x, the mean concentration was 21.4 ± 17.7 ppb. The mean concentration of
173 SO₂ was 2.89 ± 1.10 ppb. The measured mean O₃ concentration was 54.5 ± 38.8 ppb. The
174 mean PM_{2.5} concentration was 22.6 ± 16.8 µg/m³, with a maximum value of 71.8 µg/m³.
175 As for the background LJ site, The mean value of the wind speed, RH, and T were 3.13
176 m/s, 50.23%, and 6.5 °C, respectively. The mean PM_{2.5} mass concentration was $6.2 \pm$
177 5.7 µg/m³. The mean NO_x and SO₂ concentrations were 0.05 ppb and 0.97 ppb
178 respectively.

179 The characteristics of the measurement sites are summarized and shown in Fig. 1.
180 The differences in the temperature and RH among these sites mainly resulted from the
181 that the measurements were conducted in different seasons. The concentrations of SO₂,
182 NO_x, and PM_{2.5} indicated that the urban site PKU was the most polluted. The suburban
183 site CP was slightly polluted and the background LJ was the cleanest.

184 The air mass back trajectories as shown in Fig. S9 during the measurement at PKU
185 show that the measurement site was mainly influenced by the polluted air from the south
186 and southeast, and the relatively clean air from the northwest. The CP site was mainly
187 influenced by the clean air from the northwest and the polluted air from the southeast.
188 The air mass of the LJ site was mainly from the southwest and west.

189 **3.2 Mixing states of the thinly coated and thickly coated BC-containing aerosols**

190 The measured lag time probability distributions for the PKU, CP, and LJ sites are
 191 shown in Fig. 2 (a), (b), and (c), respectively. The lag time had two modes for each
 192 measurement site. The BC particles are sorted as thinly or thickly coated BC. A two
 193 log-normal distribution was used for the probability distribution of the lag time for BC-
 194 containing particles as:

$$195 \quad \text{PDF}(\Delta t) = \sum_{i=1,2} \frac{A_i}{\sqrt{2\pi} \log(\sigma_{g,i})} \exp \left[-\frac{\log(\Delta t) - \log(\Delta t_i)}{2 \log^2(\sigma_{g,i})} \right],$$

196 Where Δt is the lag time, A_i , $\sigma_{g,i}$, Δt_i are the scale factor, geometric standard
 197 deviation, and geometric mean lag time of mode i respectively. The critical lag time that
 198 distinguishes the thinly and thickly BC particles was determined by calculating the value
 199 when the probability distribution values of mode 1 and mode 2 are equal. In this study,
 200 the BC-containing aerosols with a lag time larger than $1.4 \mu\text{s}$ were classified as thickly
 201 coated particles for the LJ site. The other BC-containing aerosols were classified as
 202 thinly coated particles. Our critical lag time of $1.4 \mu\text{s}$ is smaller than the previous studies
 203 that distinguished the BC-containing aerosols between thinly coated BC and thickly
 204 coated BC with a lag time of $2 \mu\text{s}$ (Moteki and Kondo, 2007; Metcalf et al., 2012), 1.8
 205 μs (Metcalf et al., 2012), and $4.2 \mu\text{s}$ (Liu et al., 2010), which was determined by the
 206 internal setup up of the SP2. The critical lag time for the PKU and CP sites were $1.3 \mu\text{s}$
 207 and $1.7 \mu\text{s}$, respectively.

208 For each type of BC-containing aerosols, we calculated the coating thickness
 209 probabilities and the results are shown in Fig. 2(d), (e) and (f) for the PKU, CP, and LJ
 210 sites, respectively. Results showed that the BC-containing aerosols were mainly
 211 composed of thickly coated BC aerosols and thinly coated BC aerosols. The coating
 212 thickness for the thinly coated BC-containing aerosol was smaller than that of the thickly

213 coated BC-containing aerosols. However, the coating thickness of the thickly coated
214 BC-containing aerosols spread wider than that of the thinly coated ones.

215 The number fractions of the thickly coated BC-containing aerosols were
216 significantly different for different atmospheres as shown in Fig. 2 (g), (h), and (i). At
217 the polluted urban site, the number concentration of the thickly coated BC-containing
218 aerosols was comparable to that of the thinly coated BC-containing aerosols with the
219 number fractions of 56% and 44% for the thinly coated and thickly coated BC particles,
220 respectively. The number fraction of the thickly coated BC aerosols at the CP site was
221 67 %. However, the BC-containing aerosols at the background LJ site were dominated
222 by thickly coated ones with a number fraction of 81%.

223 The difference in the number fraction of the thickly coated BC particles was
224 synthetically influenced by the ambient pollution levels and the sources of the BC
225 aerosols. The suburban site CP had the largest number fraction of the thinly coated BC
226 particles. The CP site is not far from the urban, and thus the thinly coated BC particles
227 from the traffic contribute a large amount of the total ones. The urban site PKU had a
228 larger number fraction of the thickly coated BC than that of the CP site. This might be
229 resulted from the PKU site being more polluted than the CP site and then the aging
230 processing at the PKU site was faster than that at the CP site. The LJ site is far from the
231 traffic sources. The measured BC particles at the LJ site were mainly from long-range
232 transportation and experienced a long time of aging process than that at the CP and PKU
233 sites. Therefore, the BC-containing aerosols were dominated by the thickly coated ones
234 at the LJ sites.

235 We compared the number fraction of the thickly coated BC at different measurement
236 sites from literature (Ueda et al., 2016; Schwarz et al., 2008a; Wang et al., 2017c; Wang
237 et al., 2017a; Wu et al., 2017; Wang et al., 2017b; Wang et al., 2014; Huang et al., 2012;

238 Metcalf et al., 2012; Wang et al., 2016; Shiraiwa et al., 2007; Mcmeeking et al., 2012;
239 Subramanian et al., 2010; Schwarz et al., 2008b; Saha et al., 2018; Krasowsky et al.,
240 2018; Holder et al., 2014) and the results are shown in Fig. 3. The number fraction
241 values were divided into three different kinds of groups, namely the roadside, urban or
242 suburban, and background. Results from Fig. 3 show that the number fractions at the
243 roadside tend to be the lowest. These sites were close to the traffic sources and the
244 measured BC-containing aerosols were mainly from the traffic. The left part of the green
245 circles corresponds to the relatively clean urban or suburban sites with the number
246 fractions of the thickly coated BC around 30%. However, the number fractions of the
247 relative polluted urban or suburban sites had a larger number fraction of the thickly
248 coated BC around 50%. The number fractions of the thickly coated BC at the
249 background sites were the largest. Therefore, the number fractions of the thickly coated
250 BC-containing aerosols were synthetically influenced by the distance from the primary
251 source and the pollution levels of the ambient atmosphere. The number fraction of the
252 thickly coated BC-containing aerosols increased with the distance from the primary
253 emission sources and the pollution levels. Our results were consistent with the aerial
254 measurement by Metcalf et al. (2012), who found that the number fraction of the thickly
255 coated BC was 29%~41% at the top of the Los Angeles city and 47%-54% for the out
256 plume of this city.

257 For a better understanding of the source of the thinly coated and thickly coated BC,
258 we compared the number concentrations of the BC-containing aerosols with the source
259 apportionment results from the AMS data for the CP site. Among the PMF results, the
260 factor of hydrocarbon-like organic aerosol (HOA) is mainly composed of long-chain
261 hydrocarbon, and oxygenated organic aerosol (OOA) is mainly from the secondary
262 formation. HOA is mainly from the diesel exhaust, gasoline exhaust, and lubricating oil
263 emission. From Fig. 4(a), the number concentration of the thinly coated BC and mass

concentration of HOA showed good consistency, with R^2 equaling 0.69 as shown in Fig. S10, which further proved the evidence that the thinly coated BC-containing aerosols were from the traffic sources. The time series of the thickly coated BC and OOA showed good consistency as shown in Fig. 4 (b), with R^2 equaling 0.87. Therefore, the aging processing of the ambient BC was accompanied by the ambient OA. The mass concentration of OOA and the number concentration of thickly coated BC can be used as good indicators for each other.

3.3 Size distributions of the thinly coated and thickly coated BC-containing aerosols

The size distributions of the BC-containing aerosols exert a significant influence on their corresponding radiative effects (Zhao et al., 2019; Matsui et al., 2018). We calculated the number size distribution (NSD) of BC-containing aerosols for the thinly coated and thickly coated ones at different sites, and the results are shown in Fig. 5. It should be noted that the D_p in Fig. 5 corresponds to the mobility diameter from the DMA. The BC-containing aerosol NSD was further fit using the log-normal distribution.

As for the thinly coated BC-containing aerosols, the geometric mean diameters were 193, 161, and 162 nm for the PKU, CP, and LJ sites, respectively. The geometric standard deviations (GSD) of the BC-containing aerosol NSD were 1.50, 1.63, and 1.91 for the PKU, CP, and LJ sites, respectively. The GSD to some extent reflects the diversity of the BC sources. The LJ site had the largest GSD, which indicated multiple sources of thinly coated BC-containing aerosols. The LJ site was highly influenced by atmospheric transportation, due to the high altitude of this location (Zheng et al., 2017; Tan et al., 2021). Therefore, the thinly coated BC-containing aerosols could be originated from different orientations. As for the urban site PKU, the thinly coated BC aerosols were mainly from urban lifestyle emissions. Therefore, the thinly coated BC

289 aerosols at the PKU site had the lowest value of the GSD. However, the thinly coated
290 BC aerosols at the suburban site CP were influenced synthetically by urban lifestyle
291 sources and some other sources from suburban, and thus had a larger value of GSD than
292 that of PKU.

293 As for the thickly coated BC, it is obvious that they had larger diameters than those
294 of the thinly coated BC due to the coating of other non-BC components. The geometric
295 mean D_p values of the thickly coated BC were 294, 244, and 257 nm for the PKU, CP,
296 and LJ sites, respectively. The corresponding GSD values were 1.37, 1.41, and 1.46.

297 Based on the above results, the geometric mean D_p values of the thickly coated BC
298 aerosols were larger than that of the thinly coated BC aerosols by 52%, 52%, and 59%
299 for the PKU, CP, and LJ sites, respectively. The GSD values of the thickly coated BC
300 were consistent with that of the thinly coated BC with the lowest value at the PKU site
301 and highest value at the LJ site, which is consistent with the diversity of the sources of
302 BC-containing aerosols. For each site, the GSD values of the thickly coated BC aerosols
303 were smaller than that of the thinly coated ones. The GSD of BC-containing aerosols
304 tends to be smaller during the aging processing because the increment of the diameter
305 should decrease with the diameter.

306 **3.4 Size distribution of the thinly coated and thickly coated BC core**

307 The number and mass concentrations of the BC core under different mass equivalent
308 diameters were calculated and the results are shown in Fig. 6 and Table 1. It should be
309 noted here that, when it comes to the BC size distribution, the mass-equivalent diameter
310 of BC cores (D_{me}) (assuming a density of 1.8 g/cm³) was adopted in this study for direct
311 comparison with previous studies.

312 As for the number size distribution of the BC core, the geometric mean D_{me} of the
313 thinly coated BC particles were 115, 107, and 127 nm, for the PKU, CP, and LJ sites
314 respectively. The corresponding GSD values are 1.58 1.53 and 1.68, respectively. The
315 D_{me} for the thickly coated BC particles were 114, 95, and 111 nm for the PKU, CP,
316 and LJ sites respectively and the corresponding GSD values were 1.40, 1.45, and 1.43,
317 respectively. Both the GSD and the D_{me} of the thickly coated BC were smaller than
318 that of the thinly coated BC. The overall geometric mean diameter of the BC core
319 number size distributions are 114, 100, and 111 nm for the PKU, CP, and LJ sites
320 respectively.

321 There are mainly three possible reasons that may lead to the smaller geometric mean
322 diameter for the thinly coated BC than the thickly coated BC. First, the smaller BC core
323 tends to have a higher time lag as a smaller BC core will take a longer time to evaporate
324 the coating on it and thus the thinly coated particles tend to have smaller core diameters.
325 Second, it takes less time for the smaller BC particles to grow the same amount of
326 coating thickness when the increment of the BC particles was dominated by
327 condensation Thirdly, the small BC particles may have a longer life than the large BC
328 particles.

329 As for the mass size distribution of the BC core, the geometric mean D_{me} of the
330 thinly coated BC were 187, 182, and 238 nm for the PKU, CP, and LJ sites respectively
331 and the corresponding GSD values were 1.35, 1.48, and 1.47. The overall geometric
332 mean diameter of the BC core mass distributions are 172, 169, and 181 nm for the PKU,
333 CP, and LJ sites respectively. The geometric mean diameter of the BC core mass
334 distributions of 172 nm in PKU was slightly smaller than that of Liu et al. (2019a), with
335 a geometric mean diameter of 195 nm in another measurement in the urban environment

336 in Beijing and comparable to the of Zhang et al. (2018a) with a geometric mean diameter
337 of the BC core around 180 nm.

338 **3.5 Morphology of the BC-containing aerosols**

339 The time series of the number fractions of the attached BC-containing aerosols to
340 the total BC- containing aerosols (f_{attached}) are shown in Fig. 7. From Fig. 7, the f_{attached}
341 ranged between 0 and 0.21 with a mean value of $7.2 \pm 3.7\%$, $11.0 \pm 3.7\%$, and $10.1 \pm$
342 4.1% . Moteki et al. (2014) found that the f_{attached} was generally less than 0.1 in Tokyo.
343 The f_{attached} ranged between 3% and 16% in suburban London (Liu et al., 2015). A mean
344 value of 12% was found for biomass burning particles using electron microscopy (China
345 et al., 2013). Our measurement results were consistent with the previous studies. The
346 f_{attached} tend to increase with the $\text{PM}_{2.5}$ for different sites, which may indicate that the
347 attached BC-containing aerosols were generated from the coagulation of BC and non-
348 BC aerosols.

349 We calculated the f_{attached} under different aerosol diameters and the results are shown
350 in Fig. 8. There were few attached BC-containing aerosols when the diameter was
351 smaller than 250 nm with f_{attached} lowing than 2%. The f_{attached} increased with the diameter
352 for all of the measurement sites. It could reach 30% for the LJ sites. Based on the results
353 from the electron microscopy, the BC volume fractions are smaller than those of the
354 non-BC volume fractions in the attached BC aerosols (Moteki et al., 2014). The
355 increment of f_{attached} with D_p is essentially consistent with the results from Hu et al.
356 (2021a) that larger D_p contains more fractal BC, which is hard to be enveloped by
357 coatings. Our results further indicate that the attached BC aerosols were formed from
358 coagulation, as the coagulation efficiency of the two particles increased with the
359 difference between their sizes (Cai and Jiang, 2017; Kim et al., 2016; Mahfouz and
360 Donahue, 2021).

361 Under the heavier pollution, more secondary aerosol forms and more condensation
362 process would on one hand increase the coating of the previously coated BC particles,
363 which would not increase the number fraction of coated BC. On the other hand, the
364 condensation process would coat the attached BC particle and to some content would
365 lead to the transformation from the attached BC to coated BC particles. Based on our
366 measurement results, the above process of transformation from attached BC to coated
367 BC may not comparable to the process of coagulation between thinly coated BC and
368 non-BC particles, which would lead to the increment of the fraction of attached BC with
369 the pollution levels.

370 The f_{attached} under different aerosol number concentrations (N) and different ratios of
371 the BC-free aerosol number concentrations to the BC-containing aerosol number
372 concentrations are shown in Fig. 9. Results showed that the f_{attached} increased with the
373 above two factors. The results were consistent with the fact that the coagulation between
374 BC and non-BC components is more likely to happen with the increment of the BC-free
375 aerosol number concentrations. Based on the analysis above, we concluded that the
376 attached BC- containing aerosols are mainly formed through coagulation.

377 4 Conclusions

378 In this study, the BC microphysical properties were studied based on field
379 measurement using the DMA-SP2 system at the urban site PKU, suburban site CP and
380 a background site LJ in China.

381 The number fractions of the thickly coated BC-containing aerosols were 49%, 33%,
382 and 79% for the PKU, CP, and LJ sites respectively. The mass concentrations of the
383 thinly coated BC-containing aerosols showed good consistency with that of HOA,
384 which indicated that the thinly coated BC-containing aerosols were mainly generated

385 from the emission of vehicles. The thickly coated BC-containing aerosols are highly
386 correlated with the OOA.

387 The geometric diameter of the thinly coated BC-containing aerosols ranged between
388 160 nm and 200 nm, while the corresponding range was 240~300 nm for the thickly
389 coated BC-containing aerosols. The GSD of the BC-containing aerosols decreased
390 during the aging process. The corresponding mobility diameters of these thickly coated
391 (thinly coated) BC-containing aerosols were 294 (193), 244 (161), and 257 (162) nm.
392 The measured thickly coated (thinly coated) BC core number median diameters were
393 115 (114), 107 (95), and 127 (111) nm for the urban, suburban, and background sites,
394 respectively. The corresponding thickly coated (thinly coated) core mass median
395 diameters were 187 (154), 182 (146), and 238 (163) nm respectively. The mean diameter
396 of the thickly coated BC-containing aerosols was larger than that of the thinly coated
397 BC-containing aerosols, while the mean BC core diameter of the thickly coated BC-
398 containing aerosols was smaller than that of the thinly coated BC-containing aerosols.
399 There are about 10% of the BC-containing aerosols with the BC core attached to the
400 other non-BC components. We concluded that these attached BC-containing aerosols
401 were mainly generated by coagulation between the BC and non-BC components even
402 though the aging of the ambient BC aerosols was driven by condensation.

403 **Data availability.** The data is available at <https://doi.org/10.5281/zenodo.5816310>.

404 **Author contributions.** **Gang Zhao:** Conceptualization, Writing - Original Draft,
405 Visualization, Software, **Tianyi Tan:** Data Curation, Conceptualization, Visualization,
406 **Shuya Hu:** Data Curation, Conceptualization, **Zhuofei Du:** Data Curation, **Dongjie**
407 **Shang:** Data Curation, **Zhijun Wu:** Data Curation, Conceptualization, **Song Guo:** Data
408 Curation, Conceptualization, **Jing Zheng:** Data Curation, Conceptualization, **Wenfei**
409 **Zhu:** Data Curation, Conceptualization, **Mengren Li:** Data Curation, Conceptualization,

410 **Limin Zeng:** Data Curation, Conceptualization, **Min Hu:** Resources, Supervision, Data
411 Curation, Conceptualization, Revision.

412 ***Competing interests.*** The authors declare that they have no conflict of interest.

413 ***Acknowledgments.*** This work is supported by the China Postdoctoral Science
414 Foundation (2021M700192) and the National Natural Science Foundation of China
415 (91844301).

416

417 **References**

418 Bond, T. C. and Bergstrom, R. W.: Light Absorption by Carbonaceous Particles: An
419 Investigative Review, *Aerosol Sci. Technol.*, 40, 27-67, 10.1080/02786820500421521,
420 2006.

421 Bond, T. C., Doherty, S. J., Fahey, D. W., Forster, P. M., Berntsen, T., DeAngelo, B. J.,
422 Flanner, M. G., Ghan, S., Karcher, B., Koch, D., Kinne, S., Kondo, Y., Quinn, P. K.,
423 Sarofim, M. C., Schultz, M. G., Schulz, M., Venkataraman, C., Zhang, H., Zhang, S.,
424 Bellouin, N., Guttikunda, S. K., Hopke, P. K., Jacobson, M. Z., Kaiser, J. W., Klimont,
425 Z., Lohmann, U., Schwarz, J. P., Shindell, D., Storelvmo, T., Warren, S. G., and Zender,
426 C. S.: Bounding the role of black carbon in the climate system: A scientific assessment,
427 *J Geophys Res-Atmos*, 118, 5380-5552, 10.1002/jgrd.50171, 2013.

428 Cai, R. and Jiang, J.: A new balance formula to estimate new particle formation rate:
429 reevaluating the effect of coagulation scavenging, *Atmospheric Chemistry and Physics*,
430 17, 12659-12675, 10.5194/acp-17-12659-2017, 2017.

431 China, S., Mazzoleni, C., Gorkowski, K., Aiken, A. C., and Dubey, M. K.: Morphology
432 and mixing state of individual freshly emitted wildfire carbonaceous particles, *Nature*
433 *communications*, 4, 2122, 10.1038/ncomms3122, 2013.

434 Dahlkötter, F., Gysel, M., Sauer, D., Minikin, A., Baumann, R., Seifert, P., Ansmann,
 435 A., Fromm, M., Voigt, C., and Weinzierl, B.: The Pagami Creek smoke plume after
 436 long-range transport to the upper troposphere over Europe – aerosol properties
 437 and black carbon mixing state, *Atmospheric Chemistry and Physics*, 14, 6111-6137,
 438 10.5194/acp-14-6111-2014, 2014.

439 Ding, A., Huang, X., Nie, W., Sun, J., Kerminen, V.-M., Petäjä, T., Su, H., Cheng, Y.,
 440 Yang, X.-Q., Wang, M., Chi, X., Wang, J., Virkkula, A., Guo, W., Yuan, J., Wang, S.
 441 R., Zhang, R., Wu, Y., Song, Y. C., Zhu, T., Zilitinkevich, S., Kulmala, M., and Fu, C.:
 442 Enhanced haze pollution by black carbon in megacities in China, *Geophys. Res. Lett.*,
 443 43, 2873-2879, 2016.

444 Ding, S., Liu, D., Zhao, D., Hu, K., Tian, P., Zhou, W., Huang, M., Yang, Y., Wang, F.,
 445 Sheng, J., Liu, Q., Kong, S., Cui, P., Huang, Y., He, H., Coe, H., and Ding, D.: Size-
 446 Related Physical Properties of Black Carbon in the Lower Atmosphere over Beijing and
 447 Europe, *Environ Sci Technol*, 53, 11112-11121, 10.1021/acs.est.9b03722, 2019.

448 Gysel, M., Laborde, M., Olfert, J. S., Subramanian, R., and Gröhn, A. J.: Effective
 449 density of Aquadag and fullerene soot black carbon reference materials used for SP2
 450 calibration, *Atmospheric Measurement Techniques*, 4, 2851-2858, 10.5194/amt-4-
 451 2851-2011, 2011.

452 Holder, A. L., Hagler, G. S. W., Yelverton, T. L. B., and Hays, M. D.: On-road black
 453 carbon instrument intercomparison and aerosol characteristics by driving environment,
 454 *Atmospheric Environment*, 88, 183-191,
 455 <https://doi.org/10.1016/j.atmosenv.2014.01.021>, 2014.

456 Hu, K., Liu, D., Tian, P., Wu, Y., Deng, Z., Wu, Y., Zhao, D., Li, R., Sheng, J., Huang,
 457 M., Ding, D., Li, W., Wang, Y., and Wu, Y.: Measurements of the Diversity of Shape
 458 and Mixing State for Ambient Black Carbon Particles, *Geophys. Res. Lett.*, 48,
 459 10.1029/2021gl094522, 2021a.

460 Hu, S., Zhao, G., Tan, T., Li, C., Zong, T., Xu, N., Zhu, W., and Hu, M.: Current
 461 challenges of improving visibility due to increasing nitrate fraction in PM_{2.5} during the
 462 haze days in Beijing, China, *Environmental Pollution*, 290, 118032,
 463 10.1016/j.envpol.2021.118032, 2021b.

464 Hu, W., Hu, M., Hu, W.-W., Zheng, J., Chen, C., Wu, Y., and Guo, S.: Seasonal
 465 variations in high time-resolved chemical compositions, sources, and evolution of
 466 atmospheric submicron aerosols in the megacity Beijing, *Atmospheric Chemistry and*
 467 *Physics*, 17, 9979-10000, 10.5194/acp-17-9979-2017, 2017.

468 Huang, X.-F., Sun, T.-L., Zeng, L.-W., Yu, G.-H., and Luan, S.-J.: Black carbon aerosol
 469 characterization in a coastal city in South China using a single particle soot photometer,
 470 *Atmospheric Environment*, 51, 21-28, <https://doi.org/10.1016/j.atmosenv.2012.01.056>,
 471 2012.

472 Kim, Y.-h., Yiacoumi, S., Nenes, A., and Tsouris, C.: Charging and coagulation of
 473 radioactive and nonradioactive particles in the atmosphere, *Atmospheric Chemistry and*
 474 *Physics*, 16, 3449-3462, 10.5194/acp-16-3449-2016, 2016.

475 Krasowsky, T. S., McMeeking, G. R., Sioutas, C., and Ban-Weiss, G.: Characterizing
 476 the evolution of physical properties and mixing state of black carbon particles: from
 477 near a major highway to the broader urban plume in Los Angeles, *Atmos. Chem. Phys.*,
 478 18, 11991-12010, 10.5194/acp-18-11991-2018, 2018.

479 Liu, D., Allan, J. D., Young, D. E., Coe, H., Beddows, D., Fleming, Z. L., Flynn, M. J.,
 480 Gallagher, M. W., Harrison, R. M., Lee, J., Prevot, A. S. H., Taylor, J. W., Yin, J.,
 481 Williams, P. I., and Zotter, P.: Size distribution, mixing state and source apportionment
 482 of black carbon aerosol in London during wintertime, *Atmospheric Chemistry and*
 483 *Physics*, 14, 10061-10084, 10.5194/acp-14-10061-2014, 2014.

484 Liu, D., Joshi, R., Wang, J., Yu, C., Allan, J. D., Coe, H., Flynn, M. J., Xie, C., Lee, J.,
 485 Squires, F., Kotthaus, S., Grimmond, S., Ge, X., Sun, Y., and Fu, P.: Contrasting
 486 physical properties of black carbon in urban Beijing between winter and summer,

487 Atmospheric Chemistry and Physics, 19, 6749-6769, 10.5194/acp-19-6749-2019,
 488 2019a.

489 Liu, D., Flynn, M., Gysel, M., Targino, A., Crawford, I., Bower, K., Choularton, T.,
 490 Jurányi, Z., Steinbacher, M., Hüglin, C., Curtius, J., Kampus, M., Petzold, A.,
 491 Weingartner, E., Baltensperger, U., and Coe, H.: Single particle characterization of
 492 black carbon aerosols at a tropospheric alpine site in Switzerland, Atmospheric
 493 Chemistry and Physics, 10, 7389-7407, 10.5194/acp-10-7389-2010, 2010.

494 Liu, H., Pan, X., Liu, D., Liu, X., Chen, X., Tian, Y., Sun, Y., Fu, P., and Wang, Z.:
 495 Mixing characteristics of refractory black carbon aerosols determined by a tandem
 496 CPMA-SP2 system at an urban site in Beijing, Atmospheric Chemistry and Physics
 497 Discussions, 1-25, 10.5194/acp-2019-244, 2019b.

498 Liu, S., Aiken, A. C., Gorkowski, K., Dubey, M. K., Cappa, C. D., Williams, L. R.,
 499 Herndon, S. C., Massoli, P., Fortner, E. C., Chhabra, P. S., Brooks, W. A., Onasch, T.
 500 B., Jayne, J. T., Worsnop, D. R., China, S., Sharma, N., Mazzoleni, C., Xu, L., Ng, N.
 501 L., Liu, D., Allan, J. D., Lee, J. D., Fleming, Z. L., Mohr, C., Zotter, P., Szidat, S., and
 502 Prevot, A. S.: Enhanced light absorption by mixed source black and brown carbon
 503 particles in UK winter, Nature communications, 6, 8435, 10.1038/ncomms9435, 2015.

504 Mahfouz, N. G. A. and Donahue, N. M.: Technical note: The enhancement limit of
 505 coagulation scavenging of small charged particles, Atmos. Chem. Phys., 21, 3827-3832,
 506 10.5194/acp-21-3827-2021, 2021.

507 Matsui, H., Hamilton, D. S., and Mahowald, N. M.: Black carbon radiative effects
 508 highly sensitive to emitted particle size when resolving mixing-state diversity, Nature
 509 communications, 9, 3446, 10.1038/s41467-018-05635-1, 2018.

510 McMeeking, G. R., Bart, M., Chazette, P., Haywood, J. M., Hopkins, J. R., McQuaid,
 511 J. B., Morgan, W. T., Raut, J. C., Ryder, C. L., Savage, N., Turnbull, K., and Coe, H.:
 512 Airborne measurements of trace gases and aerosols over the London metropolitan region,
 513 Atmos. Chem. Phys., 12, 5163-5187, 10.5194/acp-12-5163-2012, 2012.

514 Menon, S., Hansen, J., Nazarenko, L., and Luo, Y.: Climate effects of black carbon
 515 aerosols in China and India, *Science*, 297, 2250-2253, 10.1126/science.1075159, 2002.
 516 Metcalf, A. R., Craven, J. S., Ensberg, J. J., Brioude, J., Angevine, W., Sorooshian, A.,
 517 Duong, H. T., Jonsson, H. H., Flagan, R. C., and Seinfeld, J. H.: Black carbon aerosol
 518 over the Los Angeles Basin during CalNex, *Journal of Geophysical Research:*
 519 *Atmospheres*, 117, <https://doi.org/10.1029/2011JD017255>, 2012.
 520 Moffet, R. C., and apos, Brien, R. E., Alpert, P. A., Kelly, S. T., Pham, D. Q., Gilles,
 521 M. K., Knopf, D. A., and Laskin, A.: Morphology and mixing of black carbon particles
 522 collected in central California during the CARES field study, *Atmospheric Chemistry*
 523 *and Physics*, 16, 14515-14525, 10.5194/acp-16-14515-2016, 2016.
 524 Moteki, N. and Kondo, Y.: Effects of Mixing State on Black Carbon Measurements by
 525 Laser-Induced Incandescence, *Aerosol Sci. Technol.*, 41, 398-417,
 526 10.1080/02786820701199728, 2007.
 527 Moteki, N. and Kondo, Y.: Method to measure time-dependent scattering cross sections
 528 of particles evaporating in a laser beam, *Journal of Aerosol Science*, 39, 348-364,
 529 10.1016/j.jaerosci.2007.12.002, 2008.
 530 Moteki, N. and Kondo, Y.: Dependence of Laser-Induced Incandescence on Physical
 531 Properties of Black Carbon Aerosols: Measurements and Theoretical Interpretation,
 532 *Aerosol Sci. Technol.*, 44, 663-675, Pii 924375405
 533 10.1080/02786826.2010.484450, 2010.
 534 Moteki, N., Kondo, Y., and Adachi, K.: Identification by single-particle soot photometer
 535 of black carbon particles attached to other particles: Laboratory experiments and ground
 536 observations in Tokyo, *Journal of Geophysical Research: Atmospheres*, 119, 1031-1043,
 537 <https://doi.org/10.1002/2013JD020655>, 2014.

538 Moteki, N., Kondo, Y., and Nakamura, S.-i.: Method to measure refractive indices of
 539 small nonspherical particles: Application to black carbon particles, *Journal of Aerosol*
 540 *Science*, 41, 513-521, <https://doi.org/10.1016/j.jaerosci.2010.02.013>, 2010.

541 Peng, J., Hu, M., Guo, S., Du, Z., Zheng, J., Shang, D., Levy Zamora, M., Zeng, L.,
 542 Shao, M., Wu, Y.-S., Zheng, J., Wang, Y., Glen, C. R., Collins, D. R., Molina, M. J.,
 543 and Zhang, R.: Markedly enhanced absorption and direct radiative forcing of black
 544 carbon under polluted urban environments, *Proceedings of the National Academy of*
 545 *Sciences*, 201602310, 10.1073/pnas.1602310113, 2016.

546 Ramanathan, V. and Carmichael, G.: Global and regional climate changes due to black
 547 carbon, *Nature Geoscience*, 1, 221-227, 10.1038/ngeo156, 2008.

548 Roberts, G. C., Ramana, M. V., Corrigan, C., Kim, D., and Ramanathan, V.:
 549 Simultaneous observations of aerosol-cloud-albedo interactions with three stacked
 550 unmanned aerial vehicles, *Proceedings of the National Academy of Sciences of the*
 551 *United States of America*, 105, 7370-7375, 10.1073/pnas.0710308105, 2008.

552 Saha, P. K., Khlystov, A., and Grieshop, A. P.: Downwind evolution of the volatility
 553 and mixing state of near-road aerosols near a US interstate highway, *Atmos. Chem.*
 554 *Phys.*, 18, 2139-2154, 10.5194/acp-18-2139-2018, 2018.

555 Schwarz, J. P., Spackman, J. R., Fahey, D. W., Gao, R. S., Lohmann, U., Stier, P., Watts,
 556 L. A., Thomson, D. S., Lack, D. A., Pfister, L., Mahoney, M. J., Baumgardner, D.,
 557 Wilson, J. C., and Reeves, J. M.: Coatings and their enhancement of black carbon light
 558 absorption in the tropical atmosphere, *J Geophys Res-Atmos*, 113,
 559 10.1029/2007jd009042, 2008a.

560 Schwarz, J. P., Gao, R. S., Spackman, J. R., Watts, L. A., Thomson, D. S., Fahey, D.
 561 W., Ryerson, T. B., Peischl, J., Holloway, J. S., Trainer, M., Frost, G. J., Baynard, T.,
 562 Lack, D. A., de Gouw, J. A., Warneke, C., and Del Negro, L. A.: Measurement of the
 563 mixing state, mass, and optical size of individual black carbon particles in urban and

564 biomass burning emissions, *Geophys. Res. Lett.*, 35,
 565 <https://doi.org/10.1029/2008GL033968>, 2008b.

566 Schwarz, J. P., Gao, R. S., Fahey, D. W., Thomson, D. S., Watts, L. A., Wilson, J. C.,
 567 Reeves, J. M., Darbeheshti, M., Baumgardner, D. G., Kok, G. L., Chung, S. H., Schulz,
 568 M., Hendricks, J., Lauer, A., Kärcher, B., Slowik, J. G., Rosenlof, K. H., Thompson, T.
 569 L., Langford, A. O., Loewenstein, M., and Aikin, K. C.: Single-particle measurements
 570 of midlatitude black carbon and light-scattering aerosols from the boundary layer to the
 571 lower stratosphere, *Journal of Geophysical Research*, 111, 10.1029/2006jd007076,
 572 2006.

573 Shang, D., Hu, M., Zheng, J., Qin, Y., Du, Z., Li, M., Fang, J., Peng, J., Wu, Y., Lu, S.,
 574 and Guo, S.: Particle number size distribution and new particle formation under the
 575 influence of biomass burning at a high altitude background site at Mt. Yulong (3410 m),
 576 China, *Atmospheric Chemistry and Physics*, 18, 15687-15703, 10.5194/acp-18-15687-
 577 2018, 2018.

578 Shiraiwa, M., Kondo, Y., Moteki, N., Takegawa, N., Miyazaki, Y., and Blake, D. R.:
 579 Evolution of mixing state of black carbon in polluted air from Tokyo, *Geophys. Res.*
 580 *Lett.*, 34, <https://doi.org/10.1029/2007GL029819>, 2007.

581 Subramanian, R., Kok, G. L., Baumgardner, D., Clarke, A., Shinozuka, Y., Campos, T.
 582 L., Heizer, C. G., Stephens, B. B., de Foy, B., Voss, P. B., and Zaveri, R. A.: Black
 583 carbon over Mexico: the effect of atmospheric transport on mixing state, mass
 584 absorption cross-section, and BC/CO ratios, *Atmos. Chem. Phys.*, 10, 219-237,
 585 10.5194/acp-10-219-2010, 2010.

586 Tan, T., Hu, M., Du, Z., Zhao, G., Shang, D., Zheng, J., Qin, Y., Li, M., Wu, Y., Zeng,
 587 L., Guo, S., and Wu, Z.: Measurement report: Strong light absorption induced by aged
 588 biomass burning black carbon over the southeastern Tibetan Plateau in pre-monsoon
 589 season, *Atmospheric Chemistry and Physics*, 21, 8499-8510, 10.5194/acp-21-8499-
 590 2021, 2021.

591 Ueda, S., Nakayama, T., Taketani, F., Adachi, K., Matsuki, A., Iwamoto, Y., Sadanaga,
 592 Y., and Matsumi, Y.: Light absorption and morphological properties of soot-containing
 593 aerosols observed at an East Asian outflow site, Noto Peninsula, Japan, *Atmos. Chem.*
 594 *Phys.*, 16, 2525-2541, 10.5194/acp-16-2525-2016, 2016.
 595 Ulbrich, I. M., Canagaratna, M. R., Zhang, Q., Worsnop, D. R., and Jimenez, J. L.:
 596 Interpretation of organic components from Positive Matrix Factorization of aerosol
 597 mass spectrometric data, *Atmospheric Chemistry and Physics*, 9, 2891-2918,
 598 10.5194/acp-9-2891-2009, 2009.
 599 Wang, J., Zhang, Q., Chen, M., Collier, S., Zhou, S., Ge, X., Xu, J., Shi, J., Xie, C., Hu,
 600 J., Ge, S., Sun, Y., and Coe, H.: First Chemical Characterization of Refractory Black
 601 Carbon Aerosols and Associated Coatings over the Tibetan Plateau (4730 m a.s.l),
 602 *Environmental Science & Technology*, 51, 14072-14082, 10.1021/acs.est.7b03973,
 603 2017a.
 604 Wang, Q., Huang, R. J., Cao, J., Han, Y., Wang, G., Li, G., Wang, Y., Dai, W., Zhang,
 605 R., and Zhou, Y.: Mixing State of Black Carbon Aerosol in a Heavily Polluted Urban
 606 Area of China: Implications for Light Absorption Enhancement, *Aerosol Sci. Technol.*,
 607 48, 689-697, 10.1080/02786826.2014.917758, 2014.
 608 Wang, Q., Huang, R., Zhao, Z., Cao, J., Ni, H., Tie, X., Zhu, C., Shen, Z., Wang, M.,
 609 Dai, W., Han, Y., Zhang, N., and Prevot, A. S. H.: Effects of photochemical oxidation
 610 on the mixing state and light absorption of black carbon in the urban atmosphere of
 611 China, *Environmental Research Letters*, 12, 10.1088/1748-9326/aa64ea, 2017b.
 612 Wang, Q., Huang, R.-J., Zhao, Z., Zhang, N., Wang, Y., Ni, H., Tie, X., Han, Y., Zhuang,
 613 M., Wang, M., Zhang, J., Zhang, X., Dusek, U., and Cao, J.: Size distribution and mixing
 614 state of refractory black carbon aerosol from a coastal city in South China, *Atmospheric*
 615 *Research*, 181, 163-171, <https://doi.org/10.1016/j.atmosres.2016.06.022>, 2016.
 616 Wang, Y., Liu, F., He, C., Bi, L., Cheng, T., Wang, Z., Zhang, H., Zhang, X., Shi, Z.,
 617 and Li, W.: Fractal Dimensions and Mixing Structures of Soot Particles during

618 Atmospheric Processing, *Environmental Science & Technology Letters*, 4, 487-493,
619 10.1021/acs.estlett.7b00418, 2017c.

620 Wang, Y., Hu, M., Lin, P., Tan, T., Li, M., Xu, N., Zheng, J., Du, Z., Qin, Y., Wu, Y.,
621 Lu, S., Song, Y., Wu, Z., Guo, S., Zeng, L., Huang, X., and He, L.: Enhancement in
622 Particulate Organic Nitrogen and Light Absorption of Humic-Like Substances over
623 Tibetan Plateau Due to Long-Range Transported Biomass Burning Emissions, *Environ*
624 *Sci Technol*, 53, 14222-14232, 10.1021/acs.est.9b06152, 2019a.

625 Wang, Y., Hu, M., Wang, Y., Zheng, J., Shang, D., Yang, Y., Liu, Y., Li, X., Tang, R.,
626 Zhu, W., Du, Z., Wu, Y., Guo, S., Wu, Z., Lou, S., Hallquist, M., and Yu, J. Z.: The
627 formation of nitro-aromatic compounds under high NO_x and anthropogenic VOC
628 conditions in urban Beijing, China, *Atmospheric Chemistry and Physics*, 19, 7649-7665,
629 10.5194/acp-19-7649-2019, 2019b.

630 Wilcox, E. M., Thomas, R. M., Praveen, P. S., Pistone, K., Bender, F. A. M., and
631 Ramanathan, V.: Black carbon solar absorption suppresses turbulence in the
632 atmospheric boundary layer, *Proceedings of the National Academy of Sciences*, 113,
633 11794-11799, 10.1073/pnas.1525746113, 2016.

634 Wu, Y., Wang, X., Tao, J., Huang, R., Tian, P., Cao, J., Zhang, L., Ho, K. F., Han, Z.,
635 and Zhang, R.: Size distribution and source of black carbon aerosol in urban Beijing
636 during winter haze episodes, *Atmos. Chem. Phys.*, 17, 7965-7975, 10.5194/acp-17-
637 7965-2017, 2017.

638 Zhang, F., Wang, Y., Peng, J., Chen, L., Sun, Y., Duan, L., Ge, X., Li, Y., Zhao, J., Liu,
639 C., Zhang, X., Zhang, G., Pan, Y., Wang, Y., Zhang, A. L., Ji, Y., Wang, G., Hu, M.,
640 Molina, M. J., and Zhang, R.: An unexpected catalyst dominates formation and radiative
641 forcing of regional haze, *Proceedings of the National Academy of Sciences*, 117, 3960-
642 3966, 10.1073/pnas.1919343117, 2020.

643 Zhang, R., Khalizov, A. F., Pagels, J., Zhang, D., Xue, H., and McMurry, P. H.:
644 Variability in morphology, hygroscopicity, and optical properties of soot aerosols

during atmospheric processing, *Proceedings of the National Academy of Sciences of the United States of America*, 105, 10291-10296, 10.1073/pnas.0804860105, 2008.

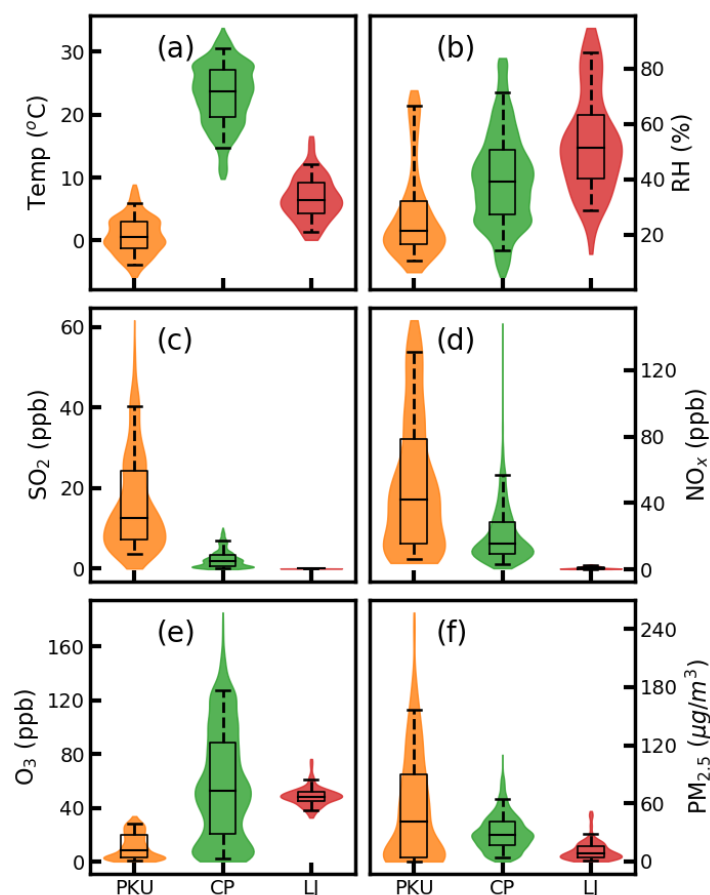
Zhang, Y., Zhang, Q., Cheng, Y., Su, H., Li, H., Li, M., Zhang, X., Ding, A., and He, K.: Amplification of light absorption of black carbon associated with air pollution, *Atmospheric Chemistry and Physics*, 18, 9879-9896, 10.5194/acp-18-9879-2018, 2018a.

Zhang, Y., Su, H., Ma, N., Li, G., Kecorius, S., Wang, Z., Hu, M., Zhu, T., He, K., Wiedensohler, A., Zhang, Q., and Cheng, Y.: Sizing of ambient particles from a Single Particle Soot Photometer measurement to retrieve mixing state of Black Carbon at a Regional site of the North China Plain, *Journal of Geophysical Research: Atmospheres*, 123, 12778-12795, doi:10.1029/2018JD028810, 2018b.

Zhao, G., Tao, J., Kuang, Y., Shen, C., Yu, Y., and Zhao, C.: Role of black carbon mass size distribution in the direct aerosol radiative forcing, *Atmos. Chem. Phys.*, 19, 13175-13188, 10.5194/acp-19-13175-2019, 2019.

Zhao, G., Hu, M., Fang, X., Tan, T., Xiao, Y., Du, Z., Zheng, J., Shang, D., Wu, Z., Guo, S., and Zhao, C.: Larger than expected variation range in the real part of the refractive index for ambient aerosols in China, *Science of The Total Environment*, 779, 146443, 10.1016/j.scitotenv.2021.146443, 2021.

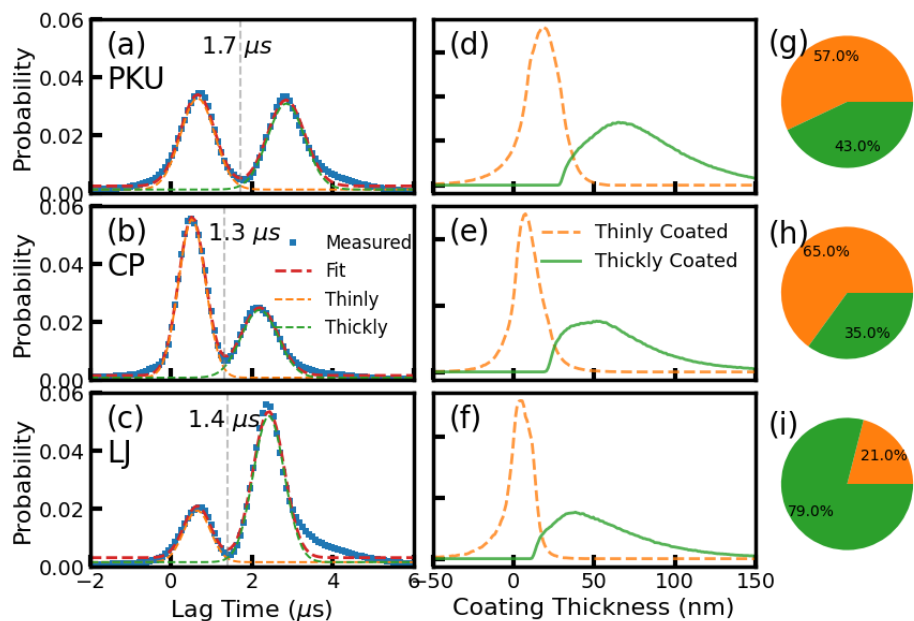
Zheng, J., Hu, M., Du, Z., Shang, D., Gong, Z., Qin, Y., Fang, J., Gu, F., Li, M., Peng, J., Li, J., Zhang, Y., Huang, X., He, L., Wu, Y., and Guo, S.: Influence of biomass burning from South Asia at a high-altitude mountain receptor site in China, *Atmospheric Chemistry and Physics*, 17, 6853-6864, 10.5194/acp-17-6853-2017, 2017.



669

670 **Figure 1.** The measured distribution of (a) temperature, (b) RH, (c) SO₂, (d) NO_x, (e)
 671 O₃ and (f) PM_{2.5} for PKU (orange), CP (green) and LJ (red) sites, respectively. The box
 672 and whisker plots represent the 5th, 25th, 75th, and 95th percentiles. The width of the
 673 filled colors represents the probability distributions of the corresponding measured
 674 values.

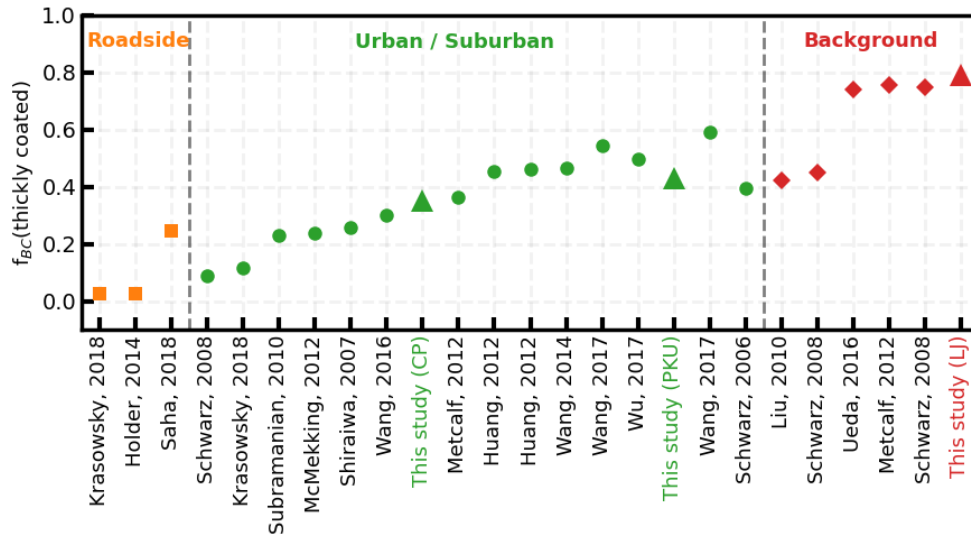
675



676

677 **Figure 2.** (a) The measured probability distribution of the lag time for the PKU site.
 678 Panel (d) shows the corresponding coating thickness distributions of thinly coated
 679 (orange) and thickly coated (green) BC-containing aerosols. Panel (g) gives the number
 680 fraction of the thinly coated (orange) and thickly coated (green) BC-containing aerosols.
 681 Panel (b), (e), and (h) are the corresponding values for the CP site. Panel (c), (f), and (g)
 682 give the results for LJ sites.

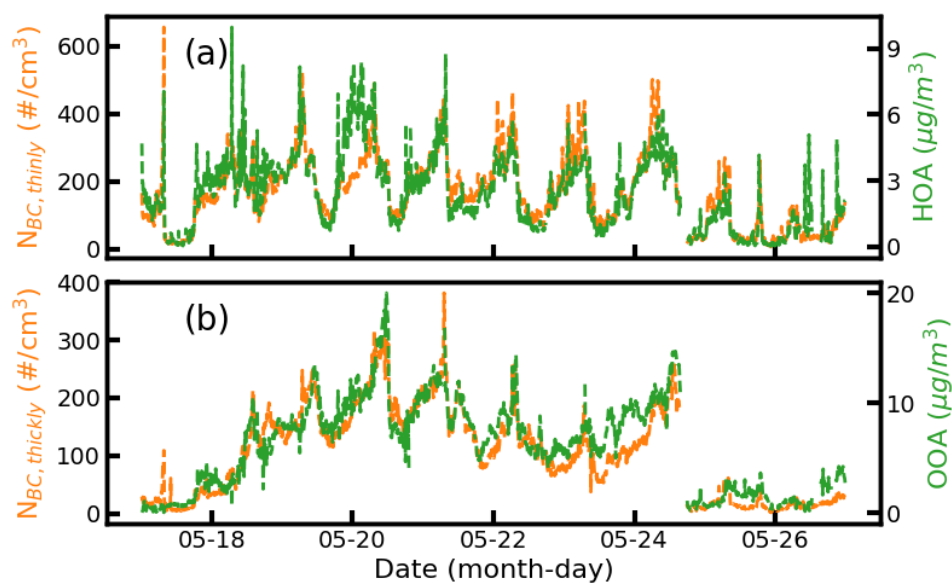
683



684

685 **Figure 3.** Measured number fraction of the thickly coated BC under different
 686 atmospheric environments based on literature. Our measured values are shown as
 687 triangles.

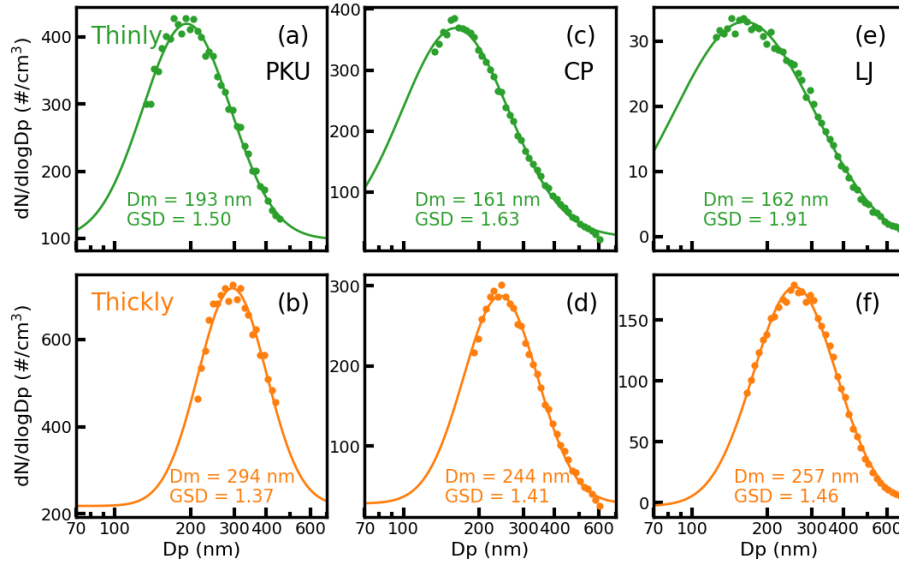
688



689

690 **Figure 4.** The time series of (a) the number concentration of the thinly coated BC
 691 (orange) and the mass concentration of HOA (green), (b) the number concentration of
 692 thickly coated BC (orange), and the mass concentration of OOA (green) for the CP site.

693



694

695 **Figure 5.** The number size distributions of the thinly coated BC-containing aerosols
 696 at (a) PKU, (c) CP, and (e) LJ sites. Panels (b), (d), and (f) are the number size
 697 distributions of the thickly coated BC-containing aerosols for the PKU, CP, and LJ sites,
 698 respectively. The dots in the figure are the measurement results and the lines are the
 699 corresponding fit results with a log-normal distribution.

700

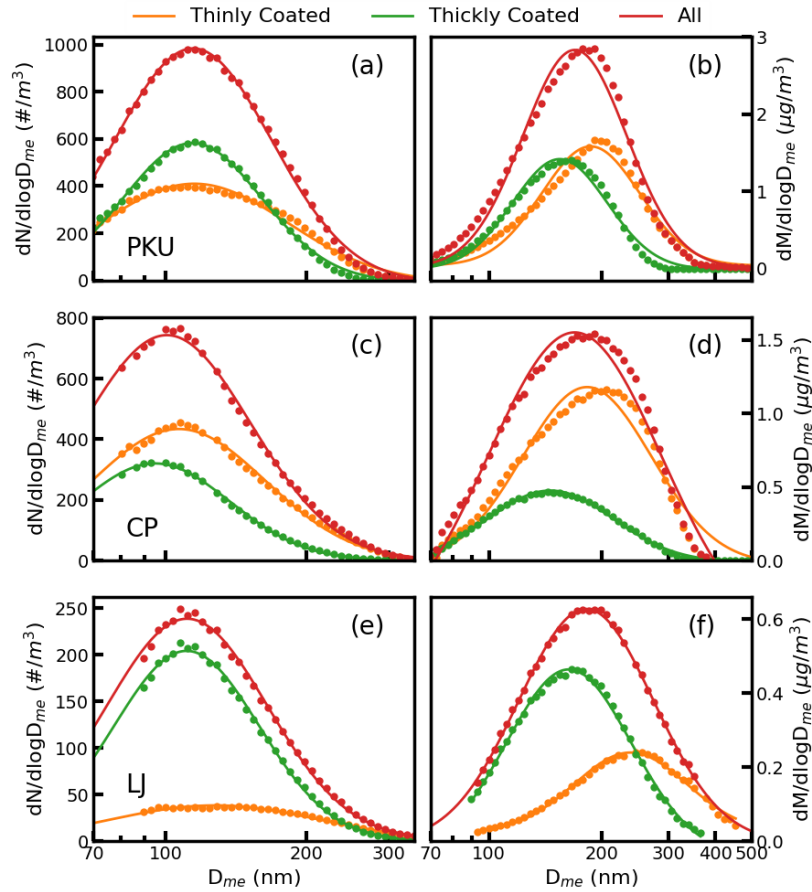
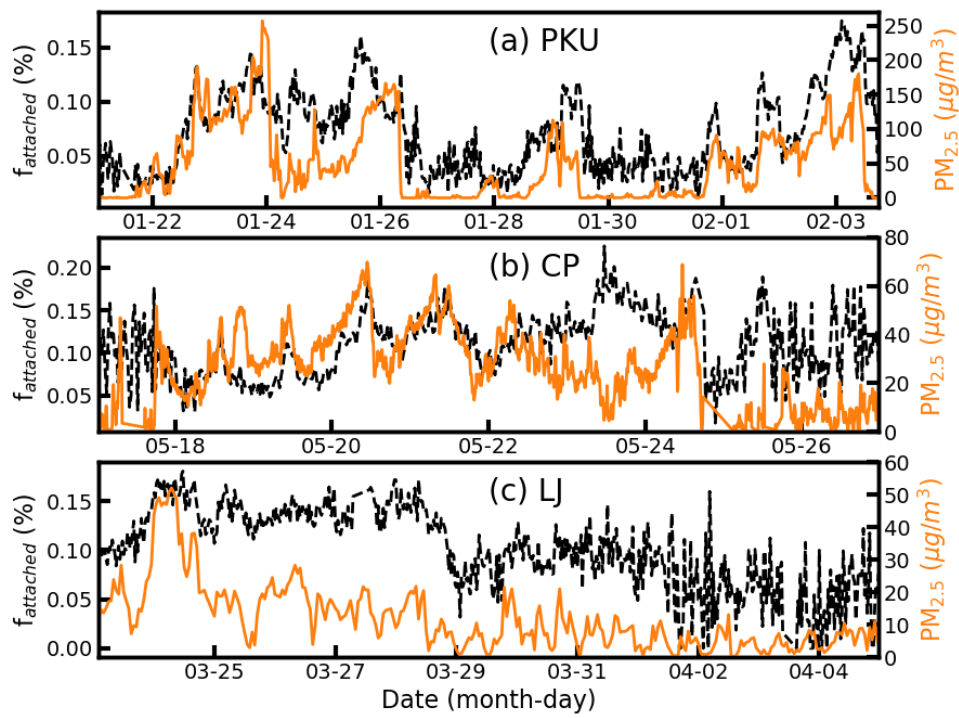


Figure 6. The BC core number size distributions of the thinly coated (orange), thickly coated (green), and overall (red) BC aerosols for the (a) PKU, (c) CP, and (e) LJ sites. Panel (b), (d) (f) show the BC core mass distributions of the thinly coated (orange), thickly coated (orange), and overall (red) BC aerosols for the PKU, CP, and LJ sites, respectively.

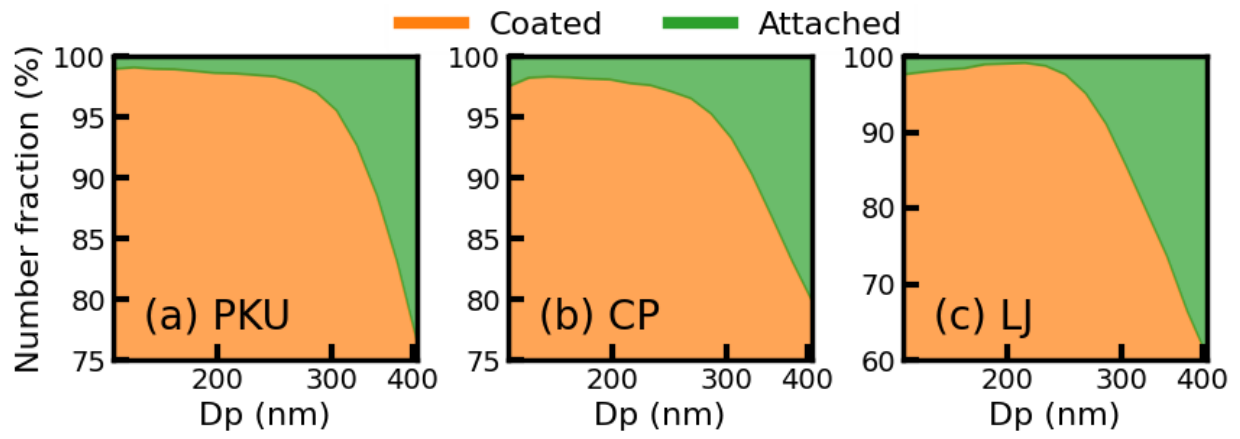


708

709 **Figure 7.** The time series of the number fractions of the attached BC (black) and $\text{PM}_{2.5}$
 710 mass concentrations (orange) for the (a) PKU, (b) CP, and (c) LJ sites.

711

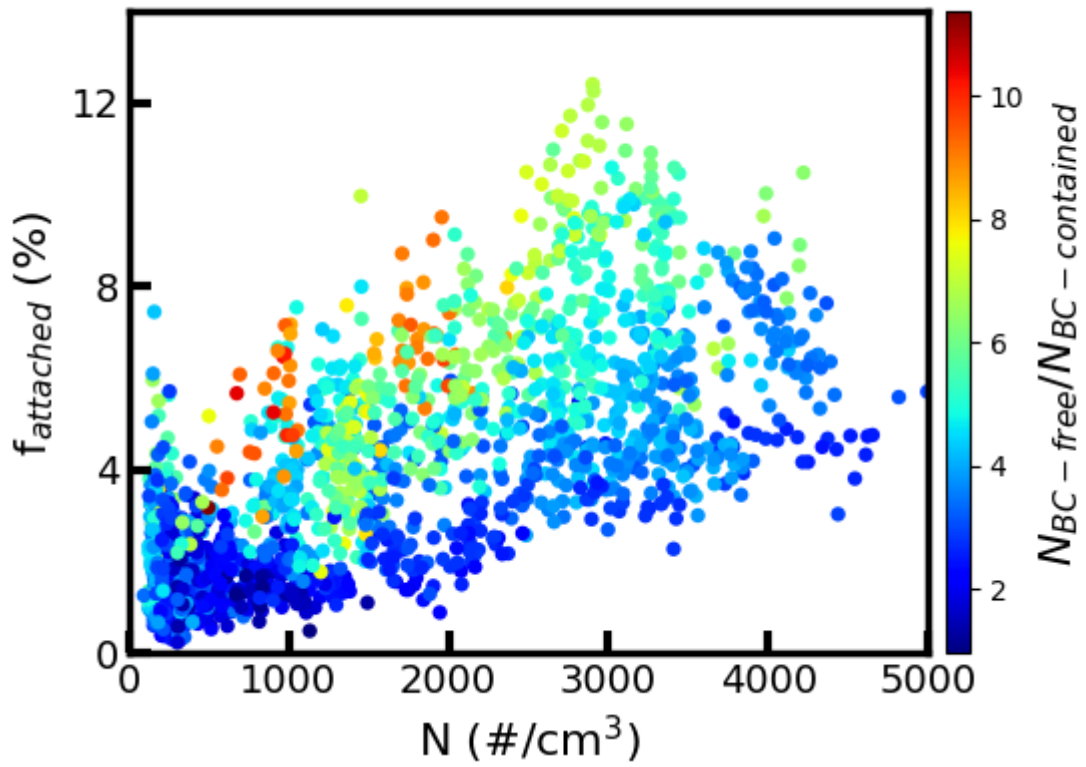
712



713

714 **Figure 8.** The number fractions of the coated and attached BC under different
715 diameters for the (a) PKU, (b) CP, and (c) LJ sites.

716



717

718 **Figure 9.** The number fractions of the attached BC aerosols under different total
 719 aerosol number concentrations for the CP sites. The filled colors represent the ratios
 720 between the BC-free aerosol number concentrations to the BC-containing aerosol
 721 number concentrations.

722

723 **Table 1.** The D_{me} and GSD values of the BC core at different sites.

Site	Value	Number Distribution			Mass Distribution ⁷²⁴		
		thinly coated	thickly coated	All	thinly coated	thickly coated	All
PKU	D_{me} (nm)	115	114	114	187	154	172
	GSD	1.58	1.40	1.47	1.35	1.34	1.37
CP	D_{me} (nm)	107	95	100	182	146	169
	GSD	1.53	1.45	1.51	1.48	1.47	1.47
LJ	D_{me} (nm)	127	111	112	238	163	181
	GSD	1.68	1.43	1.48	1.47	1.41	1.42